Smart Table Based on a Metasurface for Wireless Power Transfer

Mingzhao Song,[1,*] Kseniia Baryshnikova,[1] Aleksandr Markvart,[1] Pavel Belov,[1] Elizaveta Nenasheva,[2] Constantin Simovski,[1,3] and Polina Kapitanova[1]

[1] *Department of Nanophotonics and Metamaterials, ITMO University, Saint Petersburg 197101, Russia*
[2] *Giricond Research Institute, Ceramics Co. Ltd., Saint Petersburg 194223, Russia*
[3] *School of Electrical Engineering, Department of Electronics and Nanoengineering, Aalto University, P.O. Box 15500, FI-00076 Aalto, Finland*

(Received 28 November 2018; revised manuscript received 16 February 2019; published 16 May 2019)

We propose the concept of and experimentally demonstrate a metasurface-based smart table for wireless power transfer. The proposed structure supports propagating surface modes that can be excited by the near field of wireless devices. As a result, if two devices are placed anywhere on a metasurface table, a substantial enhancement of the effective near-field coupling can be achieved. This enhancement leads to a demonstrated power-transfer efficiency of 80% for the receiver placed in any location with respect to the transmitter on the table. The proposed concept enables a variety of applications from consumer electronics to charging electric cars.

DOI: 10.1103/PhysRevApplied.11.054046

I. INTRODUCTION

Arbitrary tailoring of electromagnetic fields is the ultimate goal in electromagnetic research from radio frequencies to optics. Metasurfaces have recently attracted a great deal of interest due to their potential to profoundly influence electromagnetic fields [1–4]. A variety of functionalities are demonstrated for a broad frequency band ranging from the microwave region to the visible region. High-impedance surfaces were initially proposed in radio-frequency and microwave regimes to reduce the antenna profile and improve radiation patterns [5]. Recently, two-dimensional artificial structures were named as metasurfaces [1], and their applications have soon spread to more-specific areas such as enhancement of magnetic resonance imaging [6]. In the optical regime, metasurfaces have paved the way for flat optics and photonics [7,8]. They can be designed to possess the required properties to replace bulky optical components. Different implementations have been demonstrated for specific purposes; for instance, a beam-focusing lens [9], a tunable lens [10], perfect absorbers [11], wavefront shapers [12], and polarizers [13].

With the proliferation of mobile electronic devices, wireless power transfer (WPT) has attracted much attention as a potential means to conveniently charge devices. Huge efforts have been made to develop different types of WPT systems [14–19]. Magnetic resonant WPT was proposed in 2007 [20], and it has become a hot research topic especially because of its potential for safe mid-range charging [21,22]. In such systems, two or more resonators with the same resonance frequency are coupled by magnetic evanescent fields. The typical charging distance is between 2 and 10 times that of the characteristic dimensions of the resonator. The charging distance is limited primarily by the inevitable evanescent-field decay rather than engineering restrictions. Thus there is little room to further extend the operation distance of a magnetic resonant WPT system in three-dimensional space. One effective approach is to increase the coupling coefficient between two distant resonators with different designs of metamaterial [23–27]. Owing to the unique property of negative permeability, such metamaterial behaves like a superlens focusing the magnetic near field generated by the transmitter and redirecting it to a receiver. Even if a metamaterial experiences intrinsic losses originating from the high current density in its resonant unit cells, it still enables a boost of power efficiency when it is placed in an optimal position between the transmitter and the receiver [26].

In contrast with metamaterials, which are three-dimensional, metasurfaces enable the manipulation of electromagnetic fields using flat and compact devices. The goal of this paper is to introduce the concept of a metasurface-based smart table for WPT applications. The smart table with a metasurface embedded in or placed underneath the desktop enables multiple devices to be powered simultaneously, regardless of where they are located on the table and how they are oriented with respect to one another [see Fig. 1(a)]. For this purpose, a metasurface can be used in different ways based on different

*kevinsmz@foxmail.com

operational principles represented by the following two examples: In Fig. 1(b), a metasurface itself plays the role of a transmitting resonator operating in a certain mode that provides a desired electromagnetic field distribution. Such a metasurface can be directly fed by a simple excitation made from an integrated electronic device. Operating in a resonant mode, the metasurface might experience high radiation losses, which can be a disadvantage of this design. In Fig. 1(c) we show another example, where a metasurface plays the role of an intermediary between the transmitter and the receiver to enhance WPT performance. The metasurface supports multiple power-transfer channels. When the existence of a receiving resonator (denoted by an orange cylinder) is detected on the metasurface, the power-transfer channel underneath is switched *on* by activation of the corresponding transmitter driven by the power divider. In this way, the electromagnetic energy can be transmitted in the form of a spatially localized surface wave that is propagating along the metasurface in a certain direction, and then coupled to the receiver. At the same time, other inactive channels remain *off*. Thus the major part of the power (denoted by I_0), which flows through the activated channel in the form of a surface wave, is much larger than the power leakage in other channels (denoted by I_1 and $I_0 >> I_1$). The advantage of this type of design is that the power can be fully exploited with minimal losses when the power-transfer channel is well designed. Here we report on a smart-table implementation based on a metasurface that serves as an intermediary between the transmitting and receiving resonators, allowing efficient WPT at distances exceeding the resonator size by an order of magnitude. To demonstrate the function of the metasurface and its possibilities for long-range power transfer, the WPT efficiency from one resonator to another is investigated both numerically and experimentally. We also evaluate the robustness of the WPT system in the presence of obstructions and calculate the specific absorption rate (SAR), which is a critical criterion for safety issues. Being low cost and compact, our design paves the way for the realization of a ubiquitous wireless charging platform.

II. DESIGN OF THE WPT SYSTEM

Wire media, arrays of parallel metal wires, have recently been studied in the microwave, terahertz, and optical frequency regimes, revealing unique electromagnetic properties [28,29]. One of these properties is the efficient conversion of evanescent waves into waves propagating in the wire medium [30–32]. This property is a key prerequisite for subwavelength imaging in wire-medium endoscopes [28,33–35]. It is also the prerequisite for efficient WPT between two resonators based on near-field coupling.

Our smart table utilizes propagating modes in a wire array to enhance the coupling between two resonators placed in the near field of the surface. For a disk resonator with colossal permittivity operating in a magnetic dipole (MD) mode, the electric field is mostly concentrated inside, while the magnetic field is maximal near the surface of the disk [36]. The evanescent tails of the magnetic field offer WPT efficiency of 50% at distances double the diameter of the resonator [36]. Increasing the distance further results in decay of efficiency. However, if a wire medium is located at a distance that is less than the resonator size, the resonator may be strongly coupled to

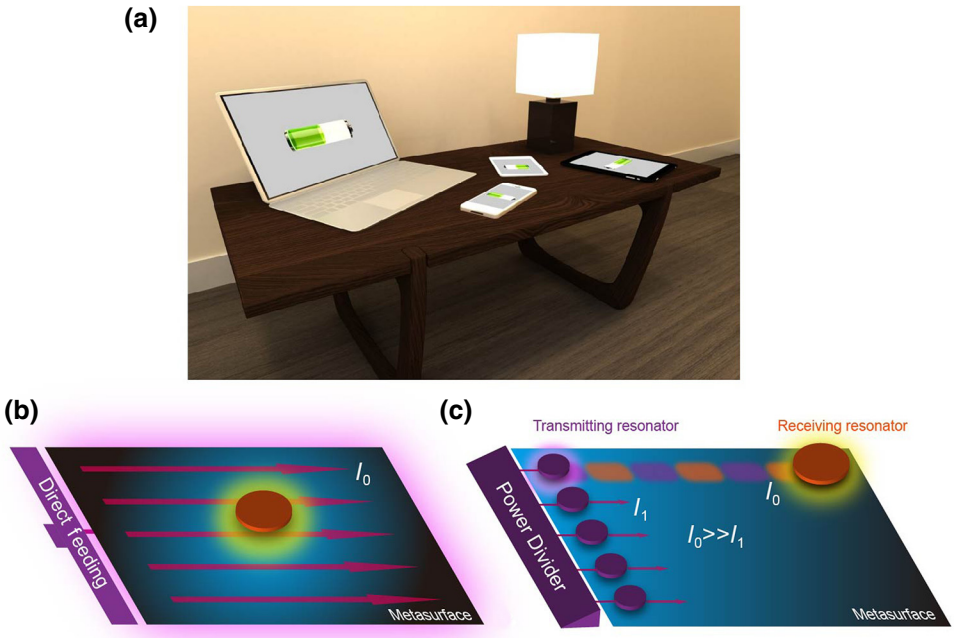

FIG. 1. Concept of smart tables based on metasurfaces. (a) Artist's view of multiple electronic devices being powered on a wireless charging table (b) Metasurface as a transmitting resonator of a WPT system. (c) Metasurface as an intermediary for enhancing WPT performance.

the wire medium. Its near magnetic field is converted into propagating modes of the wire medium, and the power can be transported from one resonator to another along the wires. Nevertheless, such a mechanism is valid for WPT because the two resonators are not electrically connected. In this work, we suggest a more-practical method than using a bulk wire medium: a metasurface of parallel wires, a planar analogue of the wire medium, is also capable of converting evanescent waves into propagating modes, and vice versa. Such an intermediary can greatly enhance coupling between distant resonators placed close to the metasurface.

The WPT system studied consists of a transmitter and a receiver placed above the metasurface as shown in Fig. 2. The transmitter comprises a dielectric disk resonator and a transmitting loop that are coaxially placed at a distance s_1 above the disk. The diameter of the dielectric disk is D and its thickness is h. The loop has diameter D_0 and is made of a conducting wire with diameter w. The receiver consists of an identical dielectric resonator and a receiving loop. The receiver is located at various distances d from the transmitter. Both the transmitter and the receiver are placed at a height s_2 above the metasurface that consists of a regular array of parallel copper wires with periods of a satisfying the criterion $w \ll a \ll \lambda$, where λ is the wavelength in free space. Three important parameters, a, N, and L, are defined by the operational principle of the proposed metasurface. Unlike conventional metasurfaces [37], where all the unit cells experience electromagnetic fields, the proposed metasurface does not operate on a certain resonant mode. Instead, only a group of wires underneath the dielectric resonators play the role of an efficient energy-transmission channel connecting the transmitter and the receiver, as depicted in Fig. 1(c). The metasurface is specially designed so that the electromagnetic fields cannot spread across the wires that are located far away from the dielectric resonators. They can only propagate along the wires as if they were guided by a quasi-transmission-line. The period a influences the characteristic impedance of this quasi-transmission-line and it also defines the coupling strength between the wires and the resonators. Figure 3 shows the simulated transmission-coefficient spectra for different periods a, which clearly demonstrate that the transmission coefficients are greater for the denser wires (corresponding to a small a), which helps create stronger coupling between the wires and the resonators. For the purpose of establishing a highly efficient WPT system, the period of the wire is chosen to be minimal, $a = 1$ cm. The total number of wires N depends on the practical needs and thus we choose $N = 18$. The wire length L has a critical impact on the system, which is discussed in the next section.

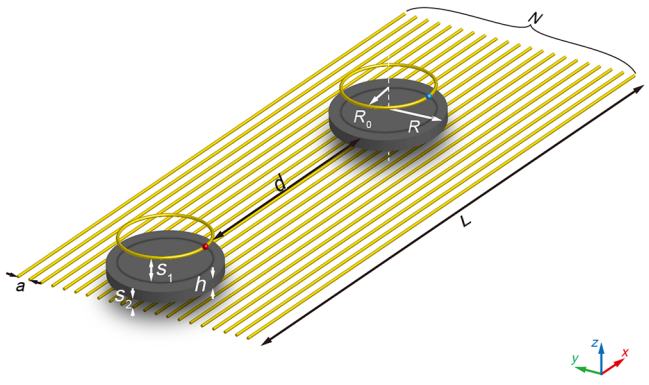

FIG. 2. Geometry of the proposed WPT system. The red and blue dots in the loop denote 50-Ω ports used in simulations and the experiment.

III. RESULTS AND DISCUSSION

A. Operational modes of the WPT system

The first issue in this study is to clarify the operational mode. Since the system incorporates several resonant objects, mode analysis needs to be performed in the first instance. We start with the eigenmode analysis of a single dielectric disk resonator, which reveals that all the magnetic modes are identified at frequencies above 230 MHz [i.e., MD, magnetic quadrupole (MQ), and magnetic octupole modes are at 232, 296, and 347 MHz, respectively], whereas all the electric modes are observed at frequencies higher than 720 MHz [i.e., electric dipole (ED) and electric quadrupole (EQ) modes are at 725 and 730 MHz, respectively]. Such a wide range of magnetic and electric eigenmode separation results from the geometric parameters of the dielectric disk resonator. Our goal is to use the MD mode of the disk, which can be excited by a

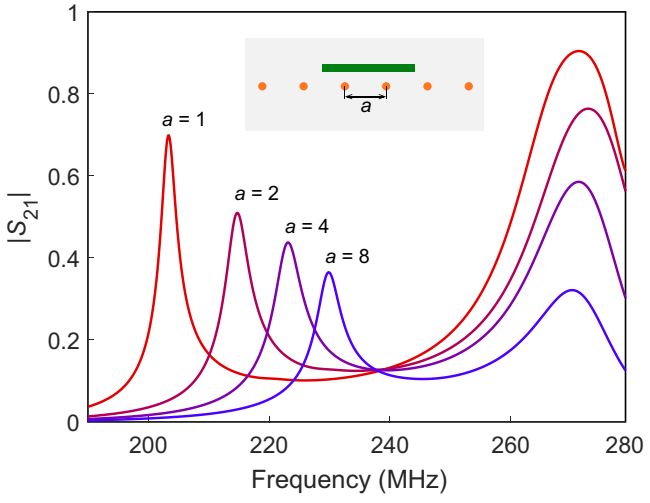

FIG. 3. Simulated transmission coefficient spectra for different wire periods a ranging from 1 to 8 cm. The inset shows a side view of the WPT system, where the other geometric parameters are fixed as $d = 25$ cm and $L = 120$ cm.

current loop [36], bearing in mind that the modes of the electric type are located far from those of the magnetic type.

The operation frequency of the WPT system should be defined in the presence of the metasurface. In the proposed WPT system, the transmitting resonator is coupled to the metasurface and, via the metasurface, to another resonator. Thus, mode frequencies in the disk resonator are shifted if the coupling between the disk and the metasurface is strong enough. Numerical simulations of the WPT system are performed with CST MICROWAVE STUDIO with use of FREQUENCY SOLVER to investigate how the wire length influences the operation frequency. We fix the distance d at 25 cm and s_2 at 1 mm and study the S parameters for different L ranging from 50 to 120 cm, as shown in the inset in Fig. 4. It can be seen how different resonances evolve as L increases: some resonances shift, whereas others remain unchanged. For instance, with $L = 120$ cm in Fig. 4 two pronounced peaks can be seen in the transmission-coefficient spectrum at 200 and 270 MHz, and for the design with $L = 50$ cm, the two peaks are observed in a similar frequency range. For a metasurface with any length L, several frequencies can always be found for efficient power transfer. However, in the case of $L = 50$ cm, the first transmission resonance shifts to 170 MHz, which is by more than 15% compared with the case of $L = 120$ cm, whereas the second transmission peak remains at a frequency of 270 MHz, it not being affected by the finite size of the metasurface. The main question that arises is then which of these two transmission peaks corresponds to the MD mode of the dielectric resonator?

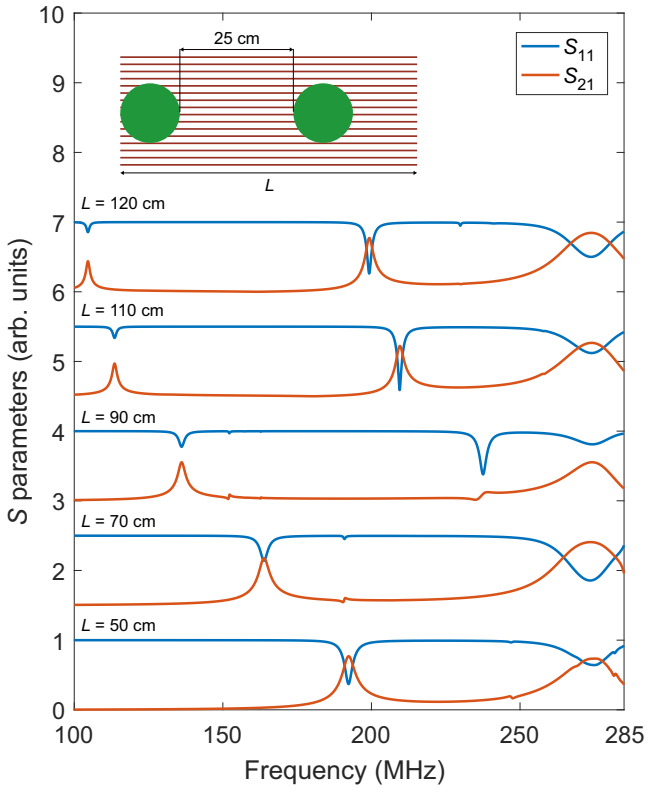

FIG. 4. Simulated S-parameter spectra for different lengths of the metasurface ranging from 50 to 120 cm. The inset shows the geometry of the system, where the distance d is fixed at 25 cm.

To clarify the nature of both resonances, we analyze the electromagnetic field distributions for the case $L = 120$ cm, as shown in Fig. 5. At 200 MHz, the electric field concentrates at the edges and in the middle of the metasurface, forming a typical standing-wave pattern. The magnetic field distribution also confirms this as a Fabry-Perot resonance of the metasurface due to its finite size. The symmetry of the standing wave is broken due to the asymmetric placement of the disks. The system is driven by the strong electric resonance of the metasurface, which allows the power transfer at this frequency.

At 270 MHz, the magnetic field is focused in the center along the axis of the dielectric disk, which is a typical feature of the MD mode. The electric and magnetic fields both remain uniform on the segment of the metasurface between the two resonators. The standing-wave features are also present on the right-hand side of the receiving resonator but they are very weak. The system is mostly driven by the magnetic response of the dielectric resonator. In the steady regime, the reactive part of the MD mode energy is stored in the disk and does not play any role, whereas the active part—with a nonzero Poynting vector—couples to the metasurface. Figures 5(b) and 5(d) show the propagation process where the active power generated by the dielectric disk resonator excites a quasi-TEM mode in the metasurface, which propagates as in a multiwire transmission line. At a distance d, this guided mode excites the same MD mode in the receiving disk. Finally, the active energy of the transmitting disk is received by the wire loop applied to the receiving disk resonator. The coupling between these objects is not of a pure electric or magnetic type, but is rather a hybrid electromagnetic coupling. The dielectric disk resonator plays a key role in this unique coupling type. First, the MD mode of the disk generates a quasi-TEM propagating mode on the metasurface through the magnetic coupling, as shown in Fig. 5(g). Second, the presence of the high-permittivity medium also guarantees an electric coupling link from the copper loop to the metasurface. In Fig. 5(f), the electric field vectors are perpendicular to the surface of the dielectric resonators, resulting in bound charges, which is clear evidence of the electric type. In this way, the hybrid electromagnetic coupling allows an efficient power transfer, since the receiver could be efficiently coupled to the metasurface at any distance from the transmitter. Therefore, in the proposed system the dielectric disk resonators cannot be replaced by conventional metallic coil resonators.

To finally clarify the mode type we perform multipole decomposition of the induced displacement currents inside

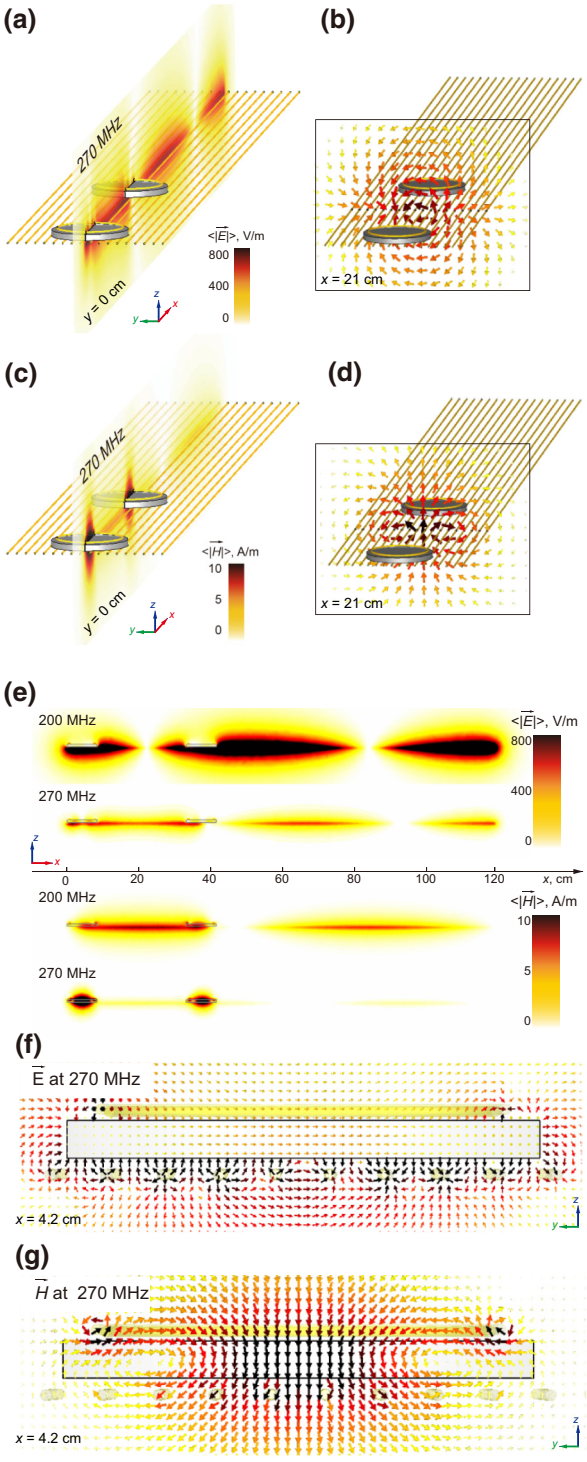

FIG. 5. Simulated electric and magnetic field distribution on different cross sections. Time-averaged (a) electric field and (c) magnetic field distribution at 270 MHz on the cross section cutting through two disk resonators (plane $y = 0$ cm). Vector form of (b) electric field and (d) magnetic field at 270 MHz on the cross section half way between two resonators (plane $x = 21$ cm). (e) Comparison of time-averaged electric and magnetic fields at 200 and 270 MHz on the plane $y = 0$ cm. Close-up view of (f) electric field and (g) magnetic field at 270 MHz on the plane $x = 4.2$ cm.

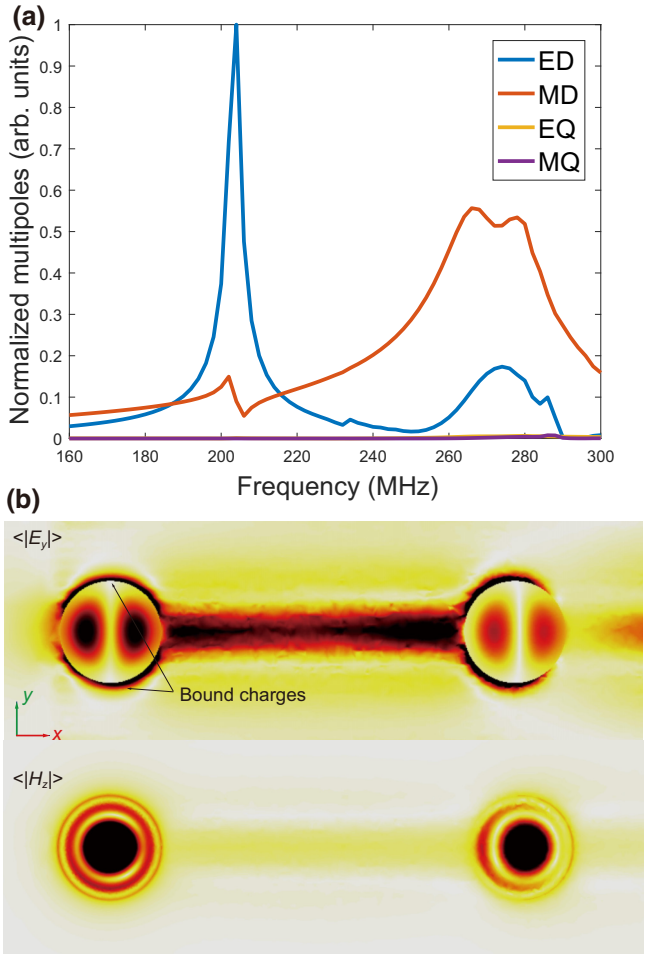

FIG. 6. (a) Multipole decomposition of the induced currents in the transmitting disk resonator. (b) E_y and H_z field distributions at 270 MHz.

the transmitting resonator. Four terms are taken into consideration; namely, ED, MD, EQ, and MQ modes [38,39]. The calculated multipoles are shown in Fig. 6(a). A strong ED mode at a frequency of 200 MHz and a MD mode at 270 MHz are observed, whereas the EQ and MQ modes do not resonate below 300 MHz and are negligibly small. However, there is also a relatively weak ED mode excited at 270 MHz. In Fig. 6(b), the generation of the MD mode can be clearly seen by the magnetic field distribution, whereas the ED mode manifests itself by the strong electric field localized at the top and bottom edges of the disks. This ED mode in the disk, which is not the eigenmode of the disk, is induced by the quasi-TEM mode on the metasurface through the electric coupling. This unique hybridization of MD and ED modes at 270 MHz is useful for WPT purposes. Thus, this frequency is defined as the operation frequency for the investigation of WPT efficiency.

B. WPT efficiency

We first demonstrate the enhanced power-transfer range near the smart table by characterizing the dependence of the efficiency on the separation distance of the resonators d. We perform numerical simulations to investigate the S-parameter spectra as a function of d ranging from 0 to 100 cm. The WPT efficiency can be calculated by $\eta = |S_{21}|^2$. Figure 7(c) shows the calculated WPT efficiency η as a function of the distance d between the transmitter and the receiver. The efficiency profile oscillates with distance due to the standing wave formed on the metasurface. A maximal WPT efficiency as high as 80% is obtained at distances $d = 25$ and 80 cm, where the magnetic field is maximal and the electric field is minimal at the center of the receiving disk. Domains where the efficiency is below 40% covered less than half of the range of possible distances. Moreover, in the regions where η is low, the magnetic field is sufficiently high for efficient WPT. At $d = 0$ and 60 cm, the ports in the transmitting and receiving loops are mismatched due to overcoupling through the metasurface, thereby leading to deep minima in efficiency. The well-known method to partially cure these minima in efficiency is to introduce matching networks [40–42].

We next experimentally study the performance of the smart table by fabricating a WPT system [see Fig. 7(a)] consisting of two identical disk resonators with $D = 84$ mm and $h = 6.6$ mm made from microwave ceramics based on a solution of $(Ba, Sr)TiO_3$ doped with Mg [43]. To excite the resonator, a nonresonant Faraday shielded loop with diameter $D_0 = 72$ mm is fabricated with use of a segment of coaxial cable. The end of each Faraday loop is connected to a 50-Ω port of an Agilent PNA E8362C vector network analyzer. The Faraday loop is coaxially placed near the resonator at a distance $s_1 = 1$ mm, the same as in the simulations. The transmitter and the receiver are both placed at a distance $s_2 = 1$ mm above the metasurface, which is fabricated as an array of copper wires with parameters as used in the simulations.

The measured S parameters as a function of frequency for d ranging from 0 to 100 cm are shown in Fig. 7(b).

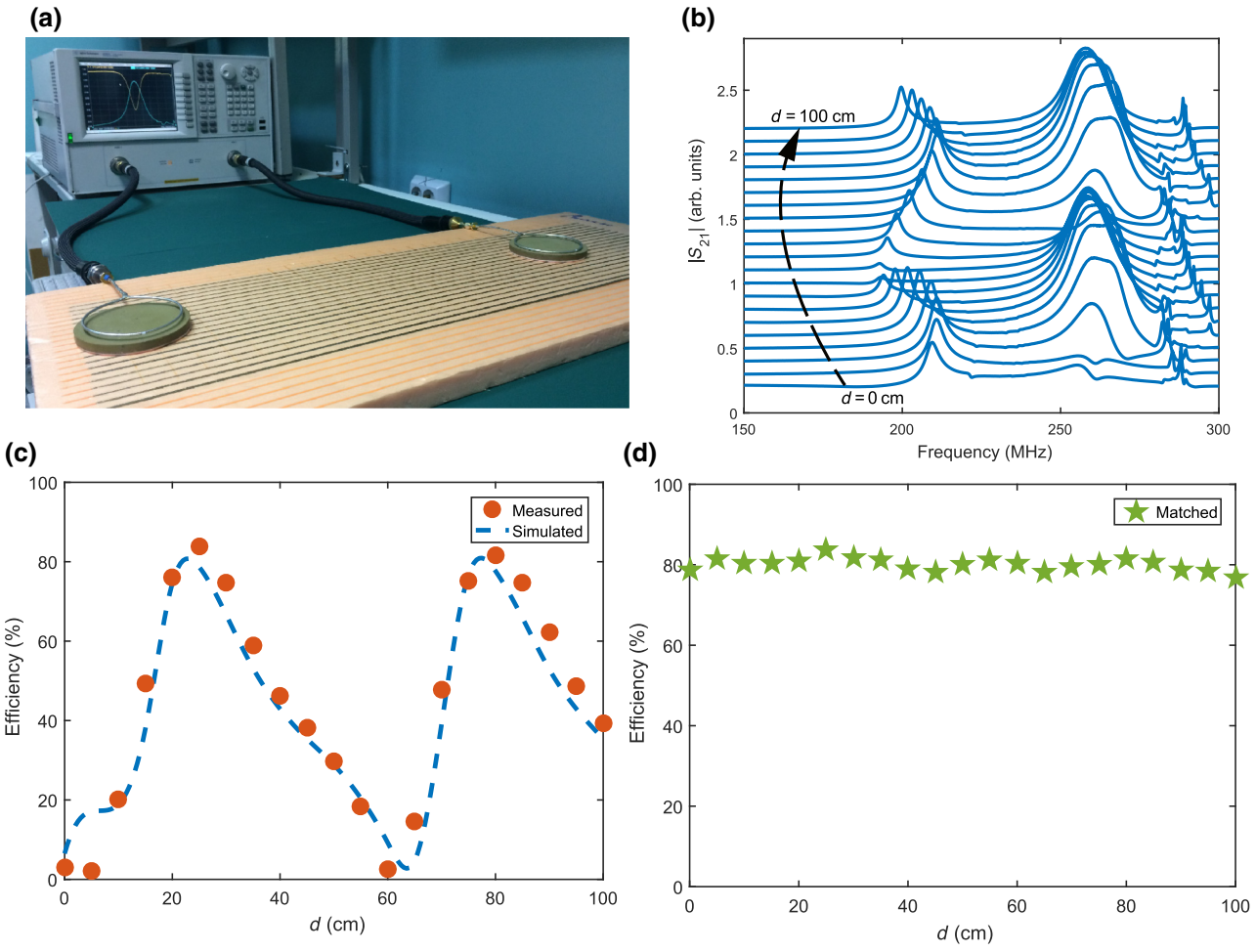

FIG. 7. (a) Photograph of the experiment setup. (b) Measured transmission-coefficient spectra for d ranging from 0 to 100 cm. (c) Comparison of measured and simulated efficiency (d) Measured WPT efficiency when both ports are matched.

The transmission spectrum S_{21} exhibits a stationary peak near 270 MHz as well as a variable peak that shifts with the separation distance d. The stationary peak is identified as corresponding to the MD resonance of the dielectric disk, which is independent of d, while the variable peak arises from the standing wave supported by the metasurface. The WPT efficiency in the MD mode is obtained from the measured S parameters and is depicted as red dots in Fig. 7(c). The maximal efficiency of 83% is obtained at $d = 25$ cm. In this work, we use a simple but effective method to match the whole system to reveal the maximal possible transfer efficiency. To match both ports, we do not insert any lumped matching circuit. Instead, at each d we mechanically tune the distances s_1 and s_2 so that $|S_{21}|$ is maximal and both $|S_{11}|$ and $|S_{22}|$ are close to zero. This method was proved to be effective in Ref. [36]. The measurements of the S parameters with this matching procedure are performed for d ranging from 0 to 100 cm with a 5-cm step, and the efficiency obtained is depicted as green stars in Fig. 7(d). The WPT efficiency is stable at $(80 \pm 3)\%$ for all distances d studied, which means that the receiver could be placed on the metasurface at any distance from the transmitter and it would be efficiently coupled to it. Moreover, the metasurface could have different dimensions. For example, the metasurface length L could be further increased to cover more area or could be decreased for customized needs. The only limitation of this WPT system is the misalignment between the transmitter and the receiver as the power channel is stretched along the metasurface. But this could be overcome by use of multiple transmitting resonators under the control of the power divider, as demonstrated in Fig. 1(b).

C. Safety issues and robustness of the system

One of the aims of the proposed WPT system is ubiquitous wireless charging. Thus, safety issues related to human exposure in electromagnetic fields and the SAR must be taken into consideration. Here we consider the SAR—a rigorous safety measurement of how much power is absorbed by biological tissues. If the proposed metasurface is used in a wireless charging system, it can be

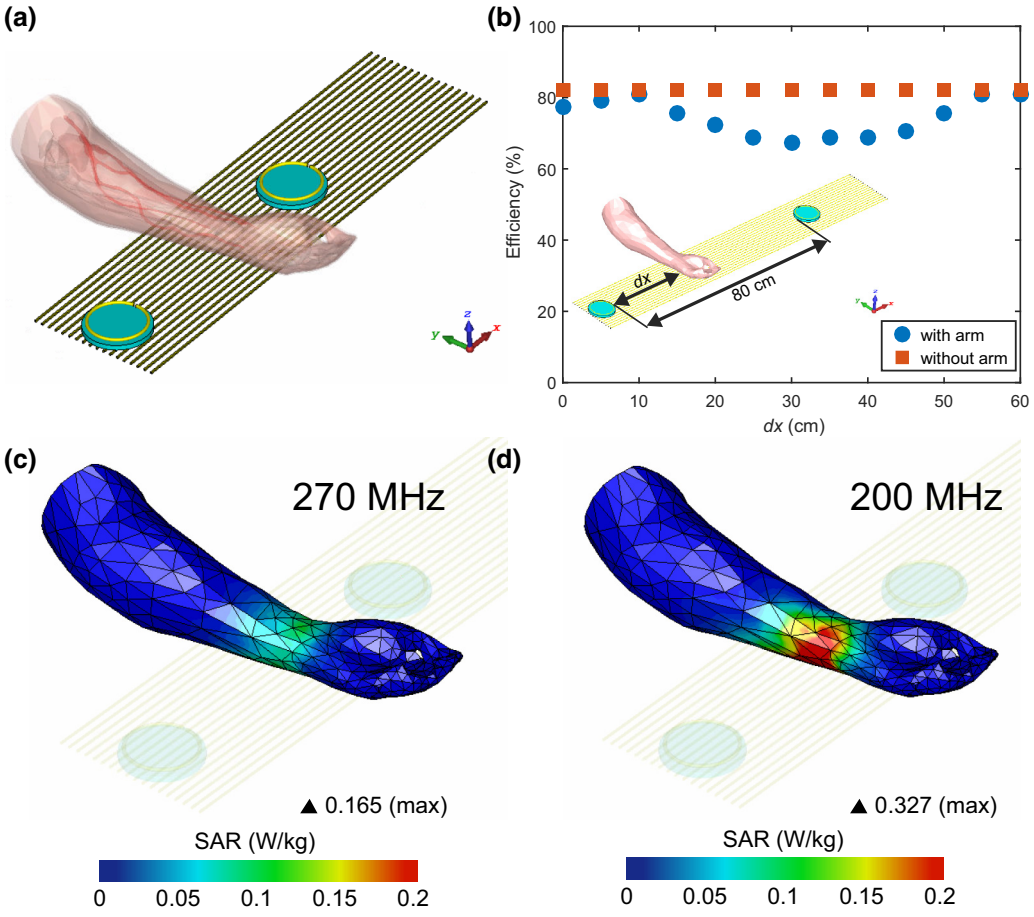

FIG. 8. (a) Simulation model of the WPT system with an arm located between the resonators 2 mm above the metasurface. (b) Simulated WPT efficiency when the obstruction (human arm) located between the resonators. Simulated SARs at the frequency of (c) the MD mode and (d) the ED mode.

embedded in a plastic or wooden desk. Thus, we consider a typical scenario in which a human arm is placed on top of the metasurface between the transmitter and the receiver. We investigate how much power can be absorbed by the human body by calculating the SAR.

To perform the SAR analysis, we use CST MICROWAVE STUDIO and a computer-aided-design model of the front part of a human arm [see Fig. 8(a)]. The model of the human arm comprises the main biological tissues of the arm (skin, fat, muscle, bone, blood, etc.), which are characterized by corresponding electromagnetic properties. The distance between the transmitter and the receiver is fixed to provide the maximal WPT efficiency without matching. The arm placed in the middle is suspended at a height of 2 mm from its bottom edge to the metasurface. For an input power of 0.5 W, the maximal SAR is 0.165 W/kg at a frequency of 270 MHz, which corresponds to the MD mode [see Fig. 8(c)]. For comparison, we also simulate the SAR at a frequency of 200 MHz (ED mode) and find that it is 0.327 W/kg, which is twice as high as for the MD mode. There are no nonlinear effects in the WPT system, and the maximal SAR for different input powers can be obtained by scaling up these results. Thus, according to an IEEE standard [44], where the SAR limit is 4.0 W/kg averaged over 10 g of tissue and absorbing most of the signal, a maximal input power of 12 W is allowed for the MD mode and only 6 W is allowed for the ED mode.

The last issue to be addressed is the robustness of the system when an obstruction is present. Here, a numerical simulation is performed to study the influence of an obstruction on the power-transfer efficiency. We consider a long-range charging scenario (i.e., the distance d between the transmitter and the receiver is 80 cm) and the human arm is placed at various distances dx to the transmitter. The simulated WPT efficiencies are shown in Fig. 8(b). It can be seen that a drop of 15 percentage points from the maximal efficiency occurred when the arm is placed in the middle.

IV. CONCLUSION

To sum up, we propose the concept of a smart table using a metasurface for wireless power transfer. We discuss two smart-table implementations based on different operational principles, where the metasurface could be used as a transmitting resonator or as an intermediary for enhanced coupling. For the latter, we fabricate the first prototype using a low-cost wire-array metasurface as an intermediary between the WPT transmitter and receiver. Numerical and experimental studies both verify efficient and distance-independent WPT. A stable WPT efficiency higher than 80% is achieved in the case where the transmitter and the receiver are both placed on the metasurface and separated by as much as 1 m. With regard to safety issues, we perform SAR analysis and demonstrate that the maximal input power of 12 W in the proposed WPT system is allowed under strict SAR regulations. We also show that the WPT system is robust when obstructions are placed between the transmitter and the receiver. The limitation of the WPT system is the misalignment between the transmitter and the receiver because the power channel is stretched along the length of the wire. This is mainly caused by the extreme anisotropy of the metasurface, and could be reduced by an isotropic metasurface design.

ACKNOWLEDGMENTS

The authors appreciate useful discussions with Georgiy Solomakha, Stanislav Glybovski, Su Xu, Mikhail Lapine, Ilya Shadrivov, and Fu Liu. The multipole-decomposition calculations were supported by the Russian Science Foundation (Grant No. 17-72-10230). The numerical simulations and the experimental investigation of the wireless-power-transfer system were supported by the Russian Science Foundation (Grant No. 17-79-20379). M.S. acknowledges support from the China Scholarship Council (Grant No. 201508090124).

[1] S. B. Glybovski, S. A. Tretyakov, P. A. Belov, Y. S. Kivshar, and C. R. Simovski, Metasurfaces: From microwaves to visible, Phys. Rep. **634**, 1 (2016).

[2] H.-T. Chen, A. J. Taylor, and N. Yu, A review of metasurfaces: Physics and applications, Rep. Prog. Phys. **79**, 076401 (2016).

[3] F. Ding, A. Pors, and S. I. Bozhevolnyi, Gradient metasurfaces: A review of fundamentals and applications, Rep. Prog. Phys. **81**, 026401 (2018).

[4] F. Liu, O. Tsilipakos, A. Pitilakis, A. C. Tasolamprou, M. S. Mirmoosa, N. V. Kantartzis, D.-H. Kwon, M. Kafesaki, C. M. Soukoulis, and S. A. Tretyakov, Intelligent Metasurfaces with Continuously Tunable Local Surface Impedance for Multiple Reconfigurable Functions, Phys. Rev. Appl. **11**, 044024 (2019).

[5] D. Sievenpiper, L. Zhang, R. F. J. Broas, N. G. Alexopolous, and E. Yablonovitch, High-impedance electromagnetic surfaces with a forbidden frequency band, IEEE Trans. Microw. Theory Tech. **47**, 2059 (1999).

[6] A. P. Slobozhanyuk, A. N. Poddubny, A. J. Raaijmakers, C. A. van Den Berg, A. V. Kozachenko, I. A. Dubrovina, I. V. Melchakova, Y. S. Kivshar, and P. A. Belov, Enhancement of magnetic resonance imaging with metasurfaces, Adv. Mater. **28**, 1832 (2016).

[7] N. Yu and F. Capasso, Flat optics with designer metasurfaces, Nat. Mater. **13**, 139 (2014).

[8] A. V. Kildishev, A. Boltasseva, and V. M. Shalaev, Planar photonics with metasurfaces, Science **339**, 1232009 (2013).

[9] M. Khorasaninejad, W. T. Chen, R. C. Devlin, J. Oh, A. Y. Zhu, and F. Capasso, Metalenses at visible wavelengths: Diffraction-limited focusing and subwavelength resolution imaging, Science **352**, 1190 (2016). http://science.sciencemag.org/content/352/6290/1190.full.pdf

[10] E. Arbabi, A. Arbabi, S. M. Kamali, Y. Horie, M. Faraji-Dana, and A. Faraon, Mems-tunable dielectric metasurface lens, Nat. Commun. **9**, 812 (2018).
[11] Y. Ra'Di, C. Simovski, and S. Tretyakov, Thin Perfect Absorbers for Electromagnetic Waves: Theory, Design, and Realizations, Phys. Rev. Appl. **3**, 037001 (2015).
[12] N. Yu, P. Genevet, M. A. Kats, F. Aieta, J.-P. Tetienne, F. Capasso, and Z. Gaburro, Light propagation with phase discontinuities: Generalized laws of reflection and refraction, Science **334**, 1210713 (2011).
[13] Y. Zhao, M. Belkin, and A. Alù, Twisted optical metamaterials for planarized ultrathin broadband circular polarizers, Nat. Commun. **3**, 870 (2012).
[14] S. Y. R. Hui, W. Zhong, and C. K. Lee, A critical review of recent progress in mid-range wireless power transfer, IEEE Trans. Power Electron. **29**, 4500 (2014).
[15] F. Lu, H. Zhang, and C. Mi, A review on the recent development of capacitive wireless power transfer technology, Energies **10**, 1752 (2017).
[16] M. Song, P. Belov, and P. Kapitanova, Wireless power transfer inspired by the modern trends in electromagnetics, Appl. Phys. Rev. **4**, 021102 (2017).
[17] S. Assawaworrarit, X. Yu, and S. Fan, Robust wireless power transfer using a nonlinear parity–time-symmetric circuit, Nature **546**, 387 (2017).
[18] A. Krasnok, D. G. Baranov, A. Generalov, S. Li, and A. Alù, Coherently Enhanced Wireless Power Transfer, Phys. Rev. Lett. **120**, 143901 (2018).
[19] M. Song, I. Iorsh, P. Kapitanova, E. Nenasheva, and P. Belov, Wireless power transfer based on magnetic quadrupole coupling in dielectric resonators, Appl. Phys. Lett. **108**, 023902 (2016).
[20] A. Kurs, A. Karalis, R. Moffatt, J. D. Joannopoulos, P. Fisher, and M. Soljačić, Wireless power transfer via strongly coupled magnetic resonances, Science **317**, 83 (2007).
[21] A. Costanzo, M. Dionigi, D. Masotti, M. Mongiardo, G. Monti, L. Tarricone, and R. Sorrentino, Electromagnetic energy harvesting and wireless power transmission: A unified approach, Proc. IEEE **102**, 1692 (2014).
[22] A. Karalis, J. D. Joannopoulos, and M. Soljačić, Efficient wireless non-radiative mid-range energy transfer, Ann. Phys. (N. Y) **323**, 34 (2008).
[23] Y. Urzhumov and D. R. Smith, Metamaterial-enhanced coupling between magnetic dipoles for efficient wireless power transfer, Phys. Rev. B **83**, 205114 (2011).
[24] W.-C. Chen, C. M. Bingham, K. M. Mak, N. W. Caira, and W. J. Padilla, Extremely subwavelength planar magnetic metamaterials, Phys. Rev. B **85**, 201104 (2012).
[25] Z. Dong, F. Yang, and J. S. Ho, Enhanced Electromagnetic Energy Harvesting with Subwavelength Chiral Structures, Phys. Rev. Appl. **8**, 044026 (2017).
[26] B. Wang, K. H. Teo, T. Nishino, W. Yerazunis, J. Barnwell, and J. Zhang, Experiments on wireless power transfer with metamaterials, Appl. Phys. Lett. **98**, 254101 (2011).
[27] J. S. Ho, B. Qiu, Y. Tanabe, A. J. Yeh, S. Fan, and A. S. Poon, Planar immersion lens with metasurfaces, Phys. Rev. B **91**, 125145 (2015).
[28] C. R. Simovski, P. A. Belov, A. V. Atrashchenko, and Y. S. Kivshar, Wire metamaterials: Physics and applications, Adv. Mater. **24**, 4229 (2012).
[29] M. A. Gorlach, M. Song, A. P. Slobozhanyuk, A. A. Bogdanov, and P. A. Belov, Topological transition in coated wire medium, Phys. Status Solidi (RRL)–Rapid Res. Lett. **10**, 900 (2016).
[30] A. Rahman, P. A. Belov, M. G. Silveirinha, C. R. Simovski, Y. Hao, and C. Parini, The importance of Fabry–Perot resonance and the role of shielding in subwavelength imaging performance of multiwire endoscopes, Appl. Phys. Lett. **94**, 031104 (2009).
[31] A. Rahman, P. A. Belov, Y. Hao, and C. Parini, Periscope-like endoscope for transmission of a near field in the infrared range, Opt. Lett. **35**, 142 (2010).
[32] P. A. Belov, G. K. Palikaras, Y. Zhao, A. Rahman, C. R. Simovski, Y. Hao, and C. Parini, Experimental demonstration of multiwire endoscopes capable of manipulating near-fields with subwavelength resolution, Appl. Phys. Lett. **97**, 191905 (2010).
[33] X. Radu, D. Garray, and C. Craeye, Toward a wire medium endoscope for mri imaging, Metamaterials **3**, 90 (2009).
[34] A. Tuniz, K. J. Kaltenecker, B. M. Fischer, M. Walther, S. C. Fleming, A. Argyros, and B. T. Kuhlmey, Metamaterial fibres for subdiffraction imaging and focusing at terahertz frequencies over optically long distances, Nat. Commun. **4**, 2706 (2013).
[35] A. Slobozhanyuk, I. Melchakova, A. Kozachenko, D. Filonov, C. Simovski, and P. Belov, An endoscope based on extremely anisotropic metamaterials for applications in magnetic resonance imaging, J. Commun. Technol. Electron. **59**, 562 (2014).
[36] M. Song, P. Belov, and P. Kapitanova, Wireless power transfer based on dielectric resonators with colossal permittivity, Appl. Phys. Lett. **109**, 223902 (2016).
[37] X. Shen, T. J. Cui, D. Martin-Cano, and F. J. Garcia-Vidal, Conformal surface plasmons propagating on ultrathin and flexible films, Proc. Natl. Acad. Sci. **110**, 40 (2013).
[38] A. B. Evlyukhin, T. Fischer, C. Reinhardt, and B. N. Chichkov, Optical theorem and multipole scattering of light by arbitrarily shaped nanoparticles, Phys. Rev. B **94**, 205434 (2016).
[39] P. D. Terekhov, K. V. Baryshnikova, Y. A. Artemyev, A. Karabchevsky, A. S. Shalin, and A. B. Evlyukhin, Multipolar response of nonspherical silicon nanoparticles in the visible and near-infrared spectral ranges, Phys. Rev. B **96**, 035443 (2017).
[40] J. O. Sophocles, *Electromagnetic Waves and Antennas* (2003), https://www.ece.rutgers.edu/~orfanidi/ewa/.
[41] C. J. Stevens, Magnetoinductive waves and wireless power transfer, IEEE Trans. Power Electron. **30**, 6182 (2015).
[42] N. Inagaki, Theory of image impedance matching for inductively coupled power transfer systems, IEEE Trans. Microw. Theory Tech. **62**, 901 (2014).
[43] E. Nenasheva, N. Kartenko, I. Gaidamaka, O. Trubitsyna, S. Redozubov, A. Dedyk, and A. Kanareykin, Low loss microwave ferroelectric ceramics for high power tunable devices, J. Eur. Ceram. Soc. **30**, 395 (2010).
[44] I. S. C. C. on Non-Ionizing Radiation Hazards, *IEEE Standard for Safety Levels with Respect to Human Exposure to Radio Frequency Electromagnetic Fields, 3 kHz to 300 GHz* (Institute of Electrical and Electronics Engineers, Incorporated, 1992).